Parallel electric fields in the upward current region of the aurora: Numerical solutions

R. E. Ergun,[a] L. Andersson, D. Main, and Y.-J. Su
Laboratory for Atmospheric and Space Physics, University of Colorado, Boulder, Colorado 80303

D. L. Newman and M. V. Goldman
Center for Integrated Plasma Studies, University of Colorado, Boulder, Colorado 80303

C. W. Carlson, J. P. McFadden, and F. S. Mozer
Space Sciences Laboratory, University of California, Berkeley, California 94720

(Received 27 March 2002; accepted 20 May 2002)

Direct observations of the parallel electric field by the Fast Auroral Snapshot satellite and the Polar satellite suggest that the ionospheric boundary of the auroral cavity is consistent with an oblique double layer that carries a substantial fraction (roughly 5% to 50%) of the auroral potential. A numerical solution to the Vlasov–Poisson equations of a planar, oblique double layer reproduces many of the properties of the observed electric fields, electron distributions, and ion distributions. The solutions indicate that the electron and ion distributions that emerge from the ionospheric side dominate the structure of the double layer. The ionospheric electron distribution includes scattered and reflected (mirrored) primaries, auroral secondaries, photoelectrons, and a cold population. A large fraction of the ionospheric electrons is reflected by the parallel electric field whereas the ionospheric ions are strongly accelerated. The steep density gradient between the ionosphere and the auroral cavity results in a highly asymmetric double layer, with a strong, localized positive charge layer on the ionospheric side and a moderate, extended negative charge layer on the auroral cavity side. This structure results in an asymmetric electric field, a feature also seen in the observations. The electric field observations, however, do not always support a planar double layer since the parallel and perpendicular signals are not always well correlated. Fully two-dimensional solutions are needed to better reproduce the observed features. © *2002 American Institute of Physics*. [DOI: 10.1063/1.1499121]

I. INTRODUCTION

One of the outstanding problems in space plasma physics has been to describe the self-consistent structure of parallel electric fields that accelerate auroral electrons. Observations from the Fast Auroral Snapshot[1] (FAST) and Polar[2] satellites have revealed new properties of the parallel electric fields and the charged particle distributions that support the existence of oblique strong double layers[3–7] at the ionospheric boundary of the auroral cavity. There has been extensive research on the topic of double layers (see Raadu[8] for a review) including an application to the auroral problem.[3–7] Thus, the theoretical framework for double layers, including oblique, strong double layers,[6,8] has been well developed.

A major advance from earlier theoretical efforts on parallel electric fields is now possible because the problem is better constrained by recent high time resolution observations.[1] Another critical advance is the recognition that a parallel electric field in the upward current region of the aurora is not confined to a single region along the auroral flux tube but, instead, there appear to be at least two spatially-separated regions of parallel electric fields. This idea is supported by recent FAST observations, earlier observations from the Dynamics Explorer satellite,[9–11] and large-scale modeling efforts.[12] The concept of several separate acceleration layers changes the modeling approach; the two regions of parallel electric fields can be treated separately. In addition, the role of wave–particle interactions, once thought to disrupt strong double layers, is now better understood with current observations. Wave emissions appear to coexist with the parallel electric field and strongly modify the accelerated distributions but do not necessarily disrupt the structure.

Our focus in this paper is to examine in detail the electric field observations, the electron distributions, and the ion distributions in the transition region between the auroral cavity and the ionosphere. Using these observations to constrain a numerical solution, we test the hypothesis that the ionosphere–auroral cavity transition region consists of an oblique double layer that carries a minority fraction of the auroral potential. We treat the two-dimensional (2-D) problem with a 1-D static Vlasov–Poisson solver. The problem is reduced to one dimension under the assumption of strong magnetization. The analysis is extended to two dimensions by treating the ion polarization and $\mathbf{E}\times\mathbf{B}$ drifts[7] as perturbations. These static solutions verify that many of the features in the observations are consistent with an oblique double layer.

[a]Also at the Department of Astrophysical and Planetary Sciences.

II. PRIOR WORK ON DOUBLE LAYERS

There has been extensive research on double layers,[8] so the theoretical development is well advanced. In this section, we do not intend to put forth a thorough review, but rather to overview the results and describe the general properties of double layers. The earliest works generally concentrated on a class of analytically-solvable, monotonic double layers. Many of these treatments assume that the electron temperatures, ion temperatures, and plasma densities are identical on both sides of the double layer. This assumption greatly simplifies the calculation and results in a high degree of symmetry in the solutions.

Two basic analytical approaches have emerged. One such approach,[13] sometimes referred to as the BGK method, has a specified monotonic potential, $\Phi(z)$, in a time-stationary, one-dimensional spatial system and all but one of the distributions (f_α for species α) are specified at the spatial boundaries. An unspecified distribution (f_u) is solved for. It must be entirely reflected or trapped and therefore it is assumed to be nonzero only in the energy range up to $|\Phi_0|$, the net potential of the double layer. The specified distributions are assumed to satisfy the time-independent Vlasov equation throughout the potential structure with f_α constant as a function of energy, ξ, from which the individual charge densities can be derived:

$$\rho_\alpha(z)=q_\alpha\int f_\alpha(\xi_\alpha(z))\left(\frac{\partial\xi_a}{\partial\nu}\right)^{-1}d\xi_\alpha, \tag{1}$$

where the energy is prescribed as

$$\xi_\alpha(z)=q_\alpha\Phi(z)+\frac{1}{2}m_a\nu^2. \tag{2}$$

A remainder function, $g(z)$, is defined:

$$g(z)=\epsilon_o\nabla^2\Phi(z)+\sum_{\alpha\neq u}\rho_\alpha(z). \tag{3}$$

In Eq. (3), the summation includes only the specified distributions so the remainder function, $g(z)$, represents the ''left over'' charge density from Poisson's equation. To satisfy Poisson's equation, the unspecified distribution (f_u) must obey the relation

$$q_u\int f_u(\xi_u(z))\left(\frac{\partial\xi_u}{\partial\nu}\right)^{-1}d\xi_u=-g(z). \tag{4}$$

Equation (4) can be inverted by analytic techniques if the potential and specified distributions are in an appropriate analytic form, otherwise a numerical solution for f_u must be found. The solution, however, must satisfy $f_u(z,\nu)\geqslant 0,\forall(z,\nu)$ to be physical. This criterion is not automatically satisfied, in fact, is difficult to satisfy, unless the potential, $\Phi(z)$, and specified distributions (f_α) are carefully constructed. We find, however, that numerical solutions can be found by using fits to auroral observations as the specified distributions and fits to auroral electric field measurements to determine the potential. It is this BGK approach that we use in this article. A complementary analytical approach involves the specification of all of the distribution functions at the boundaries and calculating the potential.[14]

Double layers have been experimentally investigated in laboratory plasmas (see Raadu[8] for a review) including strong double layers which were produced in a magnetized plasma.[15,16] A laboratory investigation of the plasma waves associated with strong double layers[17] showed a similar wave emission pattern to that which has been observed in the aurora.[1,18] In the aurora, high-frequency emissions (e.g., Langmuir and quasi-electrostatic whistler waves) are observed on the high-potential side whereas lower-frequency turbulence (e.g., ion cyclotron waves) are seen on the low-potential side.

The idea that double layers could be responsible for auroral acceleration was investigated by Block[3] who used a fluid model to construct analytic solutions. Kinetic solutions[6] later were used to model the aurora as an oblique double layer. The solutions used primarily cold species, but these studies did consider the presence of hot magnetospheric ions. Oblique double layer models assume a planar geometry and strongly magnetized electrons; electrons respond only to the parallel electric field. Ions, however, also can experience a significant polarization drift and a non-negligible portion of their energy can go into the **E×B** drift. This model was later expanded into two dimensions[8] from which solutions were found for U-shaped potential structures in accordance with early observations.[19] Oblique double layers were subsequently investigated with numerical simulations[20] that indicate that the double layer structure is nearly invariant to obliqueness of the electric field. This same numerical simulation effort concluded that the boundary conditions are critical in modeling of the auroral double layer. Thus, we emphasize the boundary condition rather than the complexities of the oblique solutions.

In this article we do not address the growth, evolution, or stability of the double layers in the aurora nor do we discuss possible nonmonotonic solutions or double layers related to ion holes.[21] A number of descriptions have been presented on the formation of double layers including ion acoustic and Bunemann instabilities. Recent efforts[22] have investigated the role of shear instabilities. This topic is best addressed by dynamic numerical simulations which can reveal the formation and evolution of the double layers as well as the interaction with nonlinear structures such as ion holes.

There has been considerable discussion on the stability of the double layers[13,23] since the Bohm condition[8] requires that the accelerated populations have drift velocities exceeding the threshold of the ion acoustic and ion cyclotron instabilities and possibly the threshold of the Bunemann instability. Strong wave emissions are associated with these unstable populations, but laboratory results have demonstrated that strong double layers are not rapidly disrupted. Auroral observations in the downward current region indicate that the wave emissions related to the double layers are spatially separated from the region of a parallel electric field.[18] Auroral observations in the upward current region, however, indicate that low-frequency waves coexist with the parallel electric field of the double layer.[1]

The role of wave–particle interactions, however, cannot be entirely ignored. The ionospheric ions, for example, are perpendicularly heated by the low-frequency turbulence and

lower hybrid waves generated by the accelerated magnetospheric electrons. The heated ions evolve into a conical distributions and acquire a significant anti-earthward drift due to the magnetic mirror force. Interestingly, this drift helps to satisfy the Bohm and Langmuir conditions[8] in a rest frame, that is, a frame with a constant altitude above the Earth's surface. Thus the double layers in the upward current region, as observed by satellites, do not appear to be moving along the magnetic field. This same ion population also experiences strong parallel heating within the double layer as it is accelerated into an ion beam. Ion heating therefore can play a significant role in the formation of the double layer. We partially account for the ion heating on the ionospheric side by using observed ionospheric ion distributions that are very near the parallel electric field.

III. OBLIQUE, ASYMMETRIC DOUBLE LAYER MODEL

The parallel electric field ($E_{\parallel}$) in the upward current region of the aurora has been modeled on a large scale with one-dimensional, quasi-neutral solutions.[12,24] These large-scale solutions with an imposed parallel potential suggest that $E_{\parallel}$ concentrates in two transition layers. The lower-altitude transition layer separates the auroral cavity, the region in between the two layers, from the ionosphere. According to the quasi-neutral model, the location and strength of the parallel potential in this layer is governed by auroral secondary electrons and the ionospheric scale height. The higher-altitude layer separates the auroral cavity from the plasma sheet-dominated magnetosphere. The auroral cavity is often dominated by an ion beam of ionospheric origin and precipitating electrons of magnetospheric origin. The current-voltage properties closely follow the Knight[25] relation. These results are supported by FAST, Polar, and Dynamics Explorer observations.

From the above modeling results and supporting observations, we now know that we can treat the parallel electric field in the transition region between the auroral cavity and the ionosphere as a separate structure from the high-altitude parallel electric field. One boundary of the transition region is the auroral cavity with electrons accelerated by a high-altitude electric field and hot magnetospheric ions that have penetrated the high-altitude potential. The other boundary of the transition region is the ionospheric plasma. Observations suggest that the double layer is oblique to the magnetic field[1,2] and carries an order of magnitude change in plasma density. The thickness of the transition region (the order of 10 km) is less than the perpendicular (to the magnetic field, **B**) width of the auroral cavity (the order of 100 km), so it appears that the planar solutions of oblique double layers may be used to reasonably model the observations.

The electric fields at the ionosphere–auroral cavity transition region display a highly asymmetric structure[1,2] with an abrupt onset on the dense ionospheric side and a more gradual relaxation in the auroral cavity. Interestingly, the Bohm condition is not met by the down-going distributions of the auroral cavity by themselves, nor is it necessary since ionospheric ions are often the majority species throughout the transition region. In addition, the electrons emerging from the ionospheric side contribute significantly ($\sim$40%) to the auroral cavity density. Thus, the ionospheric populations appear to dominate the physics of the double layer at the ionosphere–auroral cavity transition region.

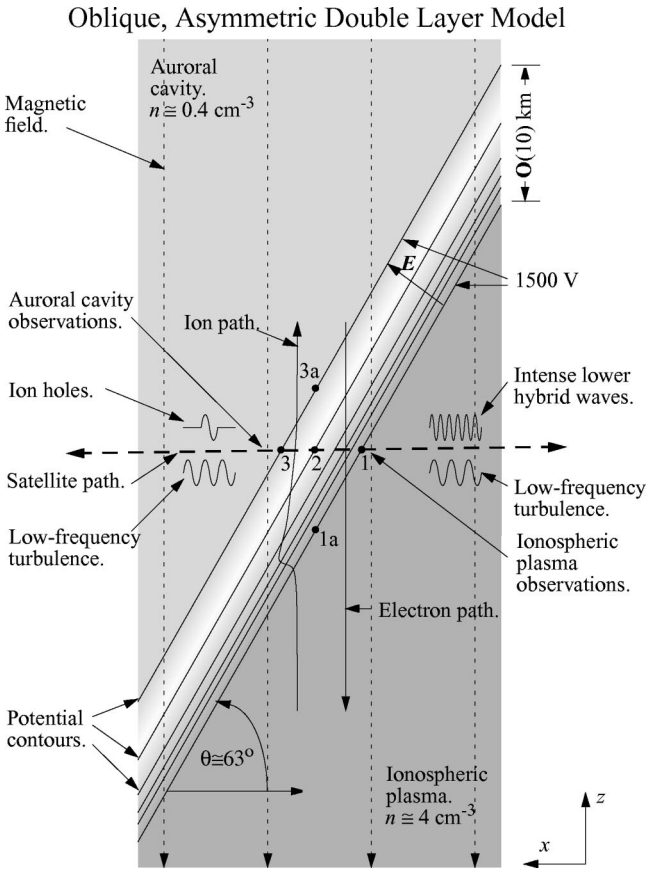

FIG. 1. A model of an oblique, asymmetric double layer. The oblique solid lines represent equipotential contours of the double layer. The vertical dashed lines indicate the magnetic field direction and the thick, horizontal dashed line is the path of a satellite traversing the region. Electrons are strongly magnetized so the electron path is guided by the magnetic field. The line labeled "ion path" includes the polarization drift of an ionospheric ion as it transits the double layer.

We label the double layer at the ionosphere–auroral cavity transition region as "strong" because the net potential $e\Phi_0 \gg T_i^{\rm is}$, $T_e^{\rm is}$, where $T_i^{\rm is}$ and $T_e^{\rm is}$ are, respectively, the ion and electron temperatures on the ionospheric (high-potential) side. The superscript "is" designates the distributions or characteristics measured on the ionospheric side of the transition region. The double layer is actually "weak" with respect to the auroral cavity parameters $e\Phi_0 \leqslant T_i^{\rm ac}$, $T_e^{\rm ac}$, where the "ac" designates the auroral cavity (low-potential side). The strong density and temperature gradients are in accordance with a highly asymmetric solution.

Figure 1 is a cartoon of a planar, oblique double layer. The vertical direction (z) represents distance along **B** (z increases with increasing altitude) and the horizontal direction (x) represents distance perpendicular to **B**. The oblique solid lines are equipotential contours of the planar double layer, assumed to extend infinitely in the $\pm y$ direction (normal to the page). The double layer is bounded on the top left by the plasma of the auroral cavity and on the bottom right by the

ionospheric plasma. The double layer carries a significant (factor of 10) density change.

We use FAST observations to constrain the boundary conditions. Ideally, it would be best to use observations separated in z along a common flux tube, but the satellite path (the dashed line in Fig. 1) is always nearly perpendicular to **B** in the auroral zone. Thus, the ionospheric plasma conditions are derived from data taken at point 1 (labeled in Fig. 1) and the auroral cavity conditions are derived from data taken at point 3. Under the assumed planar geometry, the plasma conditions at point 1 should be equivalent to those at point 1a, and likewise for points 3 and 3a. The parallel electric field ($E_\parallel$) along the satellite path should correspond to the parallel electric field along the flux tube.

The lowest-order effect (infinite magnetization) of the oblique electric field is to linearly stretch the double layer along the magnetic field by $1/\cos(\theta)$, where θ is the angle between the magnetic field (**B**) and the normal of the double layer plane. In the auroral problem, electron gyroradii are on the order of 10 meters which is far less than the double layer thickness of roughly 10 kilometers. The electron motion, therefore, is restricted to the magnetic field line (Fig. 1, electron path). The gyroradii of H^+ ions are on the order of 100 meters, so H^+ experiences a small polarization drift. Ionospheric O^+, however, can undergo a substantial polarization drift (Fig. 1, ion path) which may affect the double layer solution. The ion polarization drift was treated by Swift[7] who demonstrated that the ion density is perturbed by a factor of

$$1-\epsilon=1-\frac{e}{M\omega_{ci}^2}\frac{dE_x}{dx}, \tag{5}$$

where e is the fundamental charge, M is the ion mass, ω_{ci} the ion cyclotron frequency, and E_x is the perpendicular electric field in the x direction in Fig. 1. The net parallel energy an ion gains as it traverses the potential is reduced by $1/2M\nu_{\mathbf{E}\times\mathbf{B}}^2$ where $\nu_{\mathbf{E}\times\mathbf{B}}$ is the $\mathbf{E}\times\mathbf{B}$ drift in the y-direction. In this article, we treat the ion polarization and the $\mathbf{E}\times\mathbf{B}$ drifts as perturbations to the one-dimensional double layer problem.

IV. OBSERVATIONS AND CONSTRAINTS

We base our analysis on an event published in a companion paper[1] (Fig. 7 in that paper) which has detailed, high-resolution electron and ion distributions. The event does not completely fit the ideal model of a planar, oblique double layer since $E_\parallel$ and perpendicular ($E_\perp$) electric fields do not have a constant ratio. Nonetheless, since all of the ten reported direct observations of parallel electric fields indicate that $E_\perp > E_\parallel$ and that $E_\parallel$ and $E_\perp$ generally have a similar structure (and in some of the events have a good correlation), we proceed with a planar model for now and disregard the complexities in the observed electric field structures.

The measured parallel electric field in the event is plotted in Fig. 2(a). The horizontal axis labeled "x" is the distance that the satellite (traveling at ~ 6 km/s) traveled across the magnetic field representing observations over a 2 s period. The horizontal axis labeled "z" is the projected distance along the magnetic field assuming the geometry outlined in Fig. 1. An angle of 63° between the double layer normal and **B** is assumed. This assumption forces the net potential across the double layer, $\int_0^{24\ \mathrm{km}} E_\parallel(z)dz = 1600$ V, to be consistent with the ion beam energy. The 63° angle is also somewhat justified because it is consistent with the ratio of the peak $E_\perp$ and peak $E_\parallel$, although the two peaks are not simultaneous ($E_\perp^{\mathrm{peak}}/E_\parallel^{\mathrm{peak}} = 2.0$).

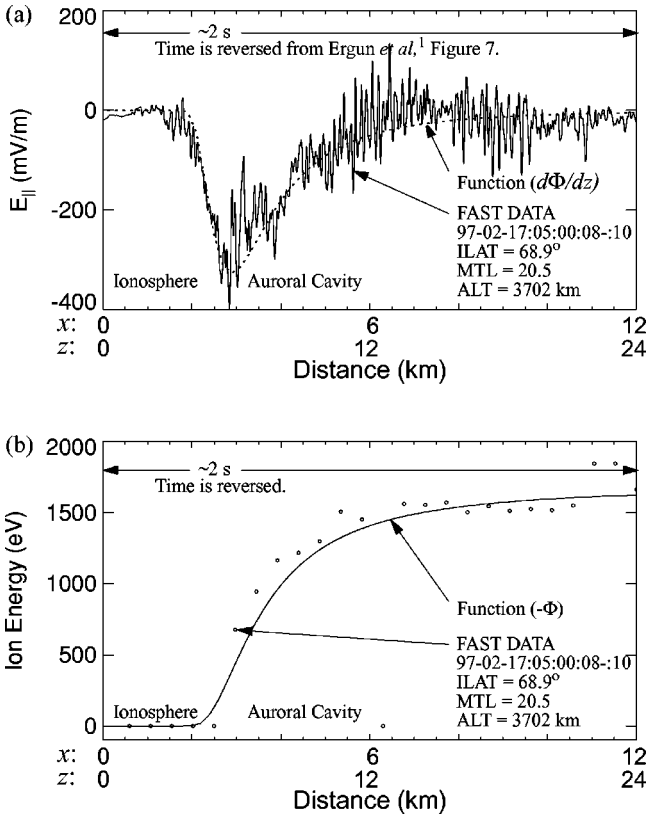

FIG. 2. (a) A magnified view (2 s) of the measured parallel electric field inside of the auroral cavity from Fig. 7 in Ergun *et al.* (Ref. 1). The horizontal axis labeled "x" is the distance the spacecraft traveled perpendicular to **B** whereas "z" is the projected distance along **B**, assuming a planar double layer diagramed in Fig. 1. The dashed line is a fit to the function $d\Phi/dz$ described in Eq. (6) with $\Phi_0 = 1600$ V and $z_0 = 4.0$ km. (b) The measured energy of the peak ion fluxes (circles) plotted against $-\Phi$.

The measured $E_\parallel$ signal [Fig. 2(a)] displays an asymmetry. It has an abrupt onset on the ionospheric side and a slow relaxation on the auroral cavity side. That asymmetric signature is seen in almost all the published events. The signal also includes a time-varying component driven by intense, low-frequency (less than the H^+ cyclotron frequency) turbulence, so a direct integration of $E_\parallel$ to determine the shape of Φ is not appropriate. Instead, we model the electric field $E_z = d\Phi/dz$ with a simple monotonic potential form:

$$\Phi(x=\mathrm{const},z) = -\Phi_0 e^{-(z_0/z)^2}, \tag{6}$$

where $\Phi_0 = 1600$ V and $z_0 = 4.0$ km. The electric field derived from Eq. (6) is drawn as a dashed line in Fig. 2. It has nearly identical amplitude and has a similar asymmetric shape as the measured signal. The potential derived from Eq. (6) also is consistent with the energy of the peak in the ion

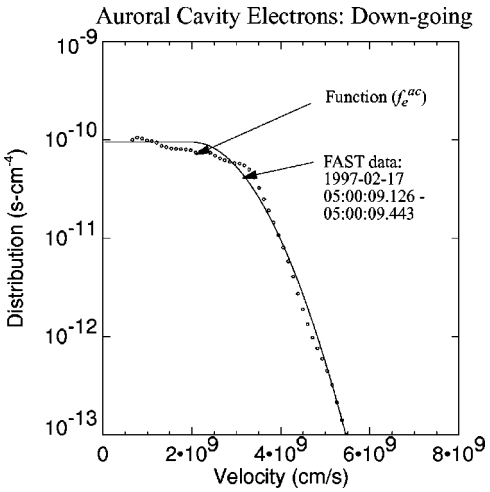

FIG. 3. The reduced, 1-D down-going electron distribution (circles) as measured by FAST in the auroral cavity immediately before crossing into the ionosphere. The solid line is a fit to the function f_e^{ac} described in Eq. (7).

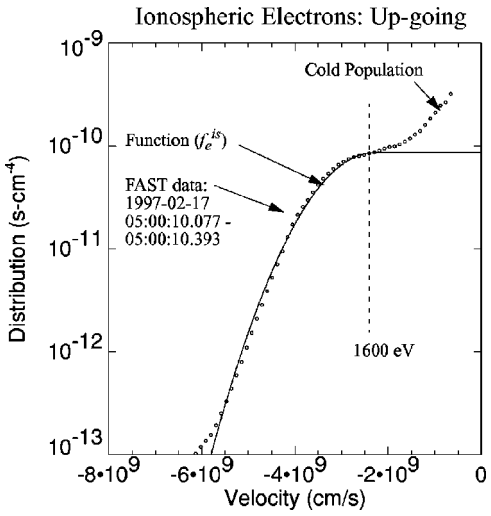

FIG. 4. The reduced, 1-D up-going electron distribution (circles) as measured by FAST in the ionosphere near the auroral cavity boundary. The solid line is a fit to the function f_e^{is} described in Eq. (7) for $\nu < 2.37\times 109$ cm/s (1600 eV).

energy flux, as shown in Fig. 2(b). The latter agreement lends support that the assumption of a planar, oblique double layer is adequate for modeling the observations.

The electron distributions and ion distributions must be specified on the high- and low-potential sides. Two of the distributions, f_i^{ac}, the auroral cavity ions and f_e^{is}, the electrons on the ionospheric side, contain particles that may be ''reflected'' or ''trapped'' (particles that have insufficient energy to pass through the structure) and particles that are ''free'' (particles that have sufficient energy to pass through the potential structure). The other two distributions, f_e^{ac}, the auroral cavity electrons and f_i^{is}, the ions on the ionospheric side, are entirely free particles streaming through the double layers. The ion distributions and the precipitating electrons (auroral cavity electrons) can be directly derived from observations.

Part of the electron distribution on the ionospheric side (f_e^{is}), however, cannot be derived from the observations since spacecraft photoelectrons contaminate the measurement at low energies (<100 eV). We therefore break this distribution into two parts. The free part of the distribution (>1600 V) is made up of precipitating electrons that were scattered or reflected in the lower ionosphere, secondary electrons emitted in the scattering process, and energetic photoelectrons produced in the ionosphere. We label the free part of the distribution as f_{ef}^{is}. This part of the distribution is specified from the observations. The reflected electron distribution (f_{er}^{is}) is numerically derived from Eq. (4). We compare the measured distributions and the derived distributions in the energy range from 100 eV to 1600 V to test the double layer solution.

As discussed above, the satellite traverses the electric field structure nearly perpendicular to **B**, so the observed auroral cavity and ionospheric distributions are not from the same flux tube. The auroral cavity electron distribution is plotted in Fig. 3. The data are from very near the ionosphere–auroral cavity transition region (Point 3 in Fig. 1, see Ergun *et al.*,[1] Fig. 7). We find that the reduced distribution is well described by a ''flat top'' distribution which we define as

$$f_e^{\mathrm{ac}}(\nu) = f_0 e^{-m_e(\nu-\nu_0)^2/2T_e^{\mathrm{ac}}} \quad (\nu \geqslant \nu_0),$$
$$f_e^{\mathrm{ac}}(\nu) = f_0 \quad (0 \leqslant \nu < \nu_0), \tag{7}$$

where m_e is the electron mass, $\nu_0 = 2.0\times 10^9$ cm/s, and T_e^{ac} (500 eV) is the plasma sheet electron temperature. Such a distribution is expected from parallel acceleration (from the high-altitude parallel electric field) and mirroring in the Earth's dipole magnetic field. The second moment of this distribution gives an effective temperature of ~ 1800 eV and an energy flux peak at 3400 eV. The value f_0 is determined by fit, and yields a density $n_e^{\mathrm{ac}} \cong 0.30$ cm^{-3} for the down-going part of the electron distribution in the auroral cavity. The analytic form will be used in the double layer solution. The auroral cavity ion distribution is modeled as a Maxwellian with $T_i^{\mathrm{ac}} = 5$ keV and $n_i^{\mathrm{ac}} \cong 0.1$ cm^{-3}, consistent with the FAST observations (see Ergun *et al.*,[1] Fig. 9).

The electron distribution on the ionospheric side is plotted in Fig. 4 along with a fit (f_{ef}^{is}) to the functional form in Eq. (7). The fit ignores the part of the measured distribution below 1600 eV (in other words, the fit is restricted to velocities $\nu < -2.37\times 10^9$ cm/s) and results in $\nu_0 = 2.3\times 10^{19}$ cm/s, $T_{ef}^{\mathrm{is}} \cong 520$ eV, and $n_{ef}^{\mathrm{is}} \cong 0.30$ cm^{-3}. The measured distribution is valid between ~ 100 eV and 1600 eV which can be compared to the solution (f_{ef}^{is}) derived from the double layer model.

Figure 5 plots the ionospheric ion distributions. The circles represent the measured distribution which indicates a cold (~ 3 eV) population with a substantial drift ($\sim 2.0\ \nu_{\mathrm{th}i}$, where $\nu_{\mathrm{th}i}$ is the ion thermal speed). The dashed line represents one count per reduced bin, that is, one count is divided equally between all the measured bins that contribute to the reduced bin. The measured ion distribution has few points that are above the one-count level per reduced bin, but does display a significant anti-earthward bulk flow.

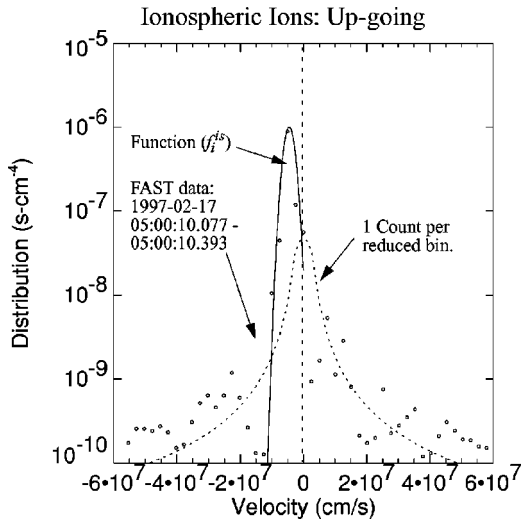

FIG. 5. The reduced, 1-D up-going ion distribution (circles) as measured by FAST in the ionosphere near the auroral cavity boundary. The solid line is a drifting Maxwellian which will be used to represent the ionospheric ion distributions. The dashed line is the 1-count level in a reduced bin.

The solid line represents a drifting Maxwellian labeled $f_i^{\rm is}$ constrained to a density $n_i^{\rm is}=4.0\ {\rm cm}^{-3}$ with $T_i^{\rm is}=3$ eV and $\nu_d=2.0\ \nu_{{\rm th}i}$:

$$f_i^{\rm is}(\nu)=f_0 e^{-M_i(\nu-\nu_d)^2/2T_i^{\rm is}}, \tag{8}$$

where M is the H^+ mass. Clearly, the ionospheric ion distribution is not as well constrained by the observations as are the electron distributions. $T_i^{\rm is}$ and ν_d are established to roughly a factor of 2.

V. NUMERICAL SOLUTIONS

Since $\Phi(z)$, $f_i^{\rm ac}$, $f_i^{\rm is}$, $f_e^{\rm ac}$, $f_{ef}^{\rm is}$ are specified by fits to observations, the reflected ionospheric electron distribution, $f_{er}^{\rm is}$, can be derived from Eq. (4). By itself, the existence of a solution $f_{er}^{\rm is}(z,\nu)\geqslant 0,\forall(z,\nu)$ will strongly support the hypothesis of an oblique double layer. Furthermore, the solution is valid for energies less than the net potential of the double layer (1600 V), so it can be compared with the observed ionospheric electron distribution in the range from 100 eV to 1600 eV. We start with the simplest case by assuming strong magnetization and the assumption of a oblique planar structure (Fig. 1). We later include the ion polarization and **E**×**B** drifts as perturbations and investigate solutions with combinations of O^+ and H^+.

A. Strongly magnetized model

The numerical solutions are obtained from a Vlasov solver with one spatial dimension and one velocity–space dimension. The spatial dimension is scaled to account for the obliqueness of the double layer. As discussed above, we assume an angle of ~63° between the double layer normal and **B**.

The basic procedures to obtain a self-consistent, time-stationary solution of double layers are well documented,[5–8,13,14] so we give a only a cursory description here. The potential, $\Phi(z)$, is prescribed from Eq. (6) on a 300 km spatial grid with variable grid spacing. The grid spacing is ~10 m on the ionospheric side and increases to ~1 km on the auroral cavity side, well below the local Debye lengths in the critical regions. The distributions, f_α, are prescribed at the boundaries of the spatial grid; the ionospheric distributions are on the left boundary, the magnetospheric distributions are on the right. The distribution functions are broken into 100 to 400 (as needed) velocity–space elements. Using the prescribed distributions at the boundaries and $\Phi(z)$, the velocity space distributions are calculated at all the spatial locations between the boundaries. Once the densities have been derived, the remainder function, $g(z)$, in Eq. (3) is determined. The reflected ionospheric electron distribution is then derived by numerically integrating Eq. (4) and solving for $f_{er}^{\rm is}$ on an energy–space grid that corresponds to each of the values Φ on the spatial grid. The distribution is then interpolated onto a velocity space grid and combined with the prescribed free ionospheric electron distribution displayed in Fig. 4.

The solution of the infinitely magnetized problem is displayed in Fig. 6 along with a table that summarizes the boundary conditions. The top panel, Fig. 6(a), plots the densities of the five species as a function of distance along **B**. Panels (b)–(d) display the potential, parallel electric field, and net charge density. Electron densities are represented by dashed lines and ion densities by solid lines. The density of the auroral cavity ions on the right boundary was increased from the observed value of $\sim 0.1\ {\rm cm}^{-3}$ to $\sim 0.15\ {\rm cm}^{-3}$ to make the right (auroral cavity) boundary charge neutral prior to solving for $g(z)$.

The auroral cavity species, prescribed on the right side, show only a small change in density. The precipitating electrons ($f_e^{\rm ac}$) have a significant acceleration from a higher-altitude parallel electric field (~3400 eV in the observations) so they are not strongly modified by the 1600 V potential. The auroral cavity ions ($f_i^{\rm ac}$) originate from the plasma sheet and thus have a high temperature and show little significant contribution to the double layer structure. The double layer solution inside the auroral cavity is substantially influenced by the ion beam (accelerated ionospheric ions) and the auroral secondary electrons.

The solution, ($f_{er}^{\rm is}$) indicates a cold, dense electron population on the ionospheric side that is reflected by the potential. Its density, the dashed line on the left side of Fig. 6(a), decreases by two orders of magnitude in ~1 km. The density of the ionospheric ions ($f_i^{\rm is}$) also decreases as the ions are accelerated into a beam. The ion density decreases slightly less rapidly than that of the cold electrons which creates the positive charge layer. The free electron population from the ionosphere ($f_{ef}^{\rm is}$) penetrates the double layer and contains ~40% of the electron density within the auroral cavity. Figure 6(a) suggests that the ionospheric ion and electron distributions dominate the physics of the double layer.

The reflected ionospheric electron distribution ($f_{er}^{\rm is}$) that was determined from the double layer solution is combined with the free electron distribution ($f_{ef}^{\rm is}$) and plotted Fig. 6(e) as a solid line. The measured electron distribution is plotted as circles. The combination of $f_{er}^{\rm is}$ and $f_{ef}^{\rm is}$ is nearly identical

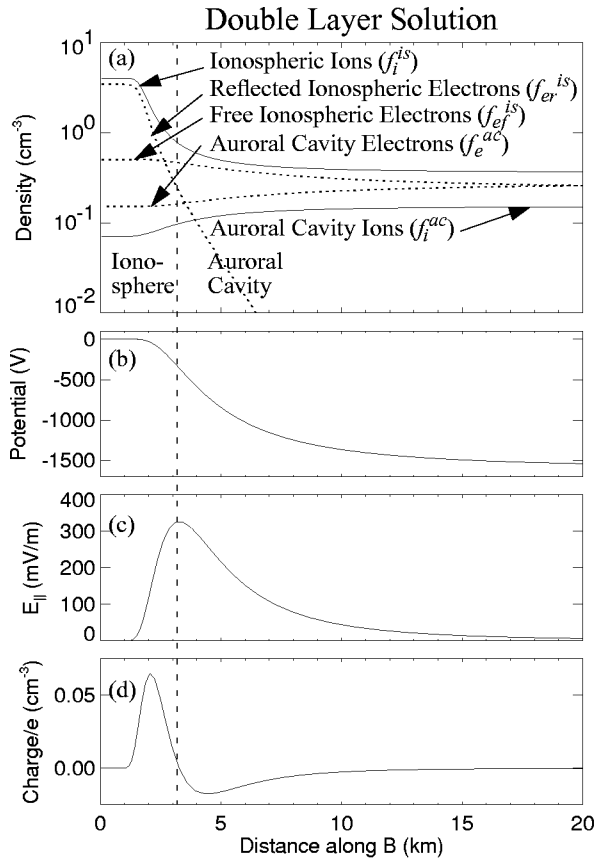

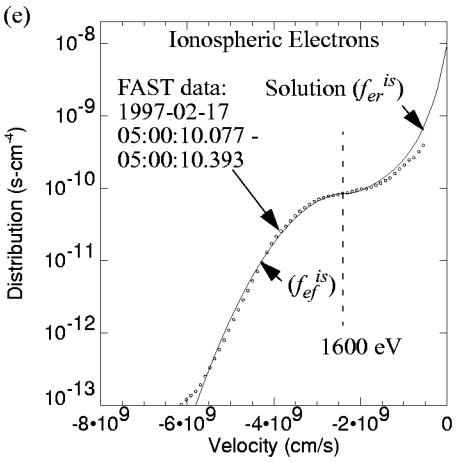

Species	Type of Fit	Den. (cm^{-3})	Temp. (eV)	Drift (v_d/v_{th})
Ionospheric Ions	Drifting Maxwellian	4.00	32	2.0
Ionospheric Electrons (>1600 eV)	Flat Top Equation 7	0.30	~1500 (500)*	-- (1.73)*
Ionospheric Electrons (≤1600 eV)	Derived	3.40	~3	--
Auroral Cavity Ions	Maxwellian	0.15	5000	--
Auroral Cavity Electrons	Flat Top Equation 7	0.30	~1800 (500)*	-- (1.5)*

* Indicates values used in Equation 7.

FIG. 6. The self-consistent numerical solution to an oblique, asymmetric double layer using fits to observed distributions. Both electrons and ions are assumed to be infinitely magnetized. (a) The densities of the ionospheric and magnetospheric populations as a function of z, the distance along **B**. (b) The electric potential, Φ. (c) The parallel electric field along **B**. The asymmetric shape in the electric field results from the strong density gradient. (d) The charge density. The double layer is, in total, charge neutral. The ionospheric side has a large but narrow ($\sim$1 km) positive charge layer. The auroral cavity side has a moderate charge layer that extends several kilometers. (e) The derived electron distribution ($<$1600 eV) and the prescribed electron distributions ($>$1600 eV). The distribution functions at the boundaries are described in the accompanying table.

to the observed distribution. Given the uncertainties in the prescribed distributions, the uncertainties in the prescribed potential, the fact that the prescribed distributions were acquired on different flux tubes, and the assumption of infinite magnetization, we find that the solution in Fig. 6 is in remarkably good agreement with the observations. This analysis supports the hypothesis that the parallel electric field at the ionospheric–auroral cavity transition region is self-consistently supported as an oblique double layer.

B. Ion polarization and E×B drifts

One of the challenges in modeling the ionospheric boundary of the auroral cavity as an oblique double layer is that the ions are not strongly magnetized,[7] particularly in the case of O^+. Fortunately, we can account for these 2-D effects by treating the polarization and **E×B** drifts as perturbations to the ionospheric ion density in the 1-D problem.[7]

The polarization drift perturbation ϵ in Eq. (5) has an absolute maximum value of $\epsilon \cong 0.05$ for H^+ ions and $\epsilon \cong 0.8$ for O^+ ions. The polarization drift for O^+ therefore is not adequately described by a first-order expansion for the prescribed potential that we derived from the observations. Instead, we use a more exact expression for the density change under the guiding center approximation derived in Appendix A:

$$\frac{n_p \nu_p}{n_u \nu_u} = \sqrt{\left(1 - \frac{e}{M\omega_{ci}^2}\frac{dE_x}{dx}\right)^2 + \left(\frac{e}{M\omega_{ci}^2}\frac{dE_x}{dz}\right)^2}, \tag{9}$$

where n_u and ν_u are the unperturbed density and velocity and n_p and ν_p are the density and velocity perturbed by the polarization and **E×B** drifts. Equation (9) reduces to Eq. (5) in the limit of $\epsilon \ll 1$.

The **E×B** drift in the y-direction reduces the net parallel energy gained from the potential (in the direction of travel) by $1/2 M v_{\mathbf{E\times B}}^2$. Including the energy of the **E×B** drift in Eq. (9), the ionospheric ion density is modified by

$$\frac{n_p \nu_p}{n_u \nu_u} = \sqrt{\left(1 - \frac{e}{M\omega_{ci}^2}\frac{dE_x}{dx}\right)^2 + \left(\frac{e}{M\omega_{ci}^2}\frac{dE_x}{dz}\right)^2} \times \sqrt{\frac{K_0 - e\Phi}{K_0 - e\Phi + 1/2M(E_x/B)^2}}, \tag{10}$$

where K_0 is the initial ion kinetic energy. This perturbation can be introduced into the one-dimensional solution.

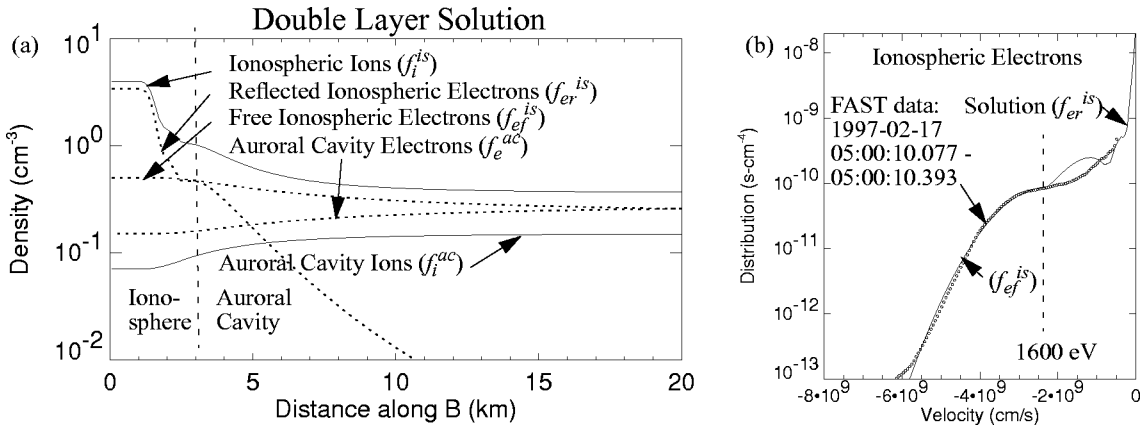

FIG. 7. The self-consistent numerical solution to an oblique, asymmetric double layer using fits to observed distributions. (a) The densities as a function of z, the distance along **B**. (b) The derived electron distribution. In this example, electrons are assumed to be infinitely magnetized. The ions are assumed to be weakly magnetized O^+. The polarization drift and the **E×B** drift are treated as perturbations using Eq. (10).

If H^+ is the dominant ionospheric constituent, n_p/n_u is near unity and the solution for the densities and the cold ionospheric electron distribution cannot be visibly distinguished from those plotted in Fig. 6. The perturbation to the O^+ plasma density, however, is quite strong, so the O^+ solutions somewhat differ from the strongly magnetized case. Figure 7 plots the solution for O^+ ionospheric ions using the perturbation described in Eq. (10). The ion density in Fig. 7(a) drops more abruptly at the ionospheric side of the double layer than in Fig. 6(a). As a result, the calculated electron distribution plotted in Fig. 7(b) has an enhancement in phase-space density at $v \cong -1.5\times10^{-9}$ cm/s and a depletion at $v \cong 0.8\times10^{-9}$ cm/s.

Figure 8 displays the solution for ionospheric ions of 50% H^+ and 50% O^+. This ratio is roughly consistent with the FAST ion mass spectrometer observations (20 second average). The O^+ ions were treated as weakly magnetized [Eq. (10)]. The predicted electron distributions are slightly greater than the observed distributions at $v \cong -1.5\times10^{-9}$ cm/s but the 50% H^+/50% O^+ solution results with a better agreement between the measured ionospheric electron distribution and the solution at low energies ($v > -1.0\times10^{-9}$ cm/s) than seen in Fig. 6 (100% H^+). Testing ratios in steps of 10%, we found that a 70% H^+/30% O^+ solution results with the least deviation in the 100 eV to 1600 eV range.

Figure 8 illustrates the effect of the polarization and **E×B** drifts. The ionospheric O^+ density (thin, solid line) in Fig. 8(a) decreases more abruptly than does the H^+ density (thick line) at $z=2$ km, primarily due to the polarization drift. The O^+ density then nearly plateaus at $z=3$ km due to the **E×B** drift. The net effect of the O^+ behavior on the solution [Fig. 8(b)] is to cause an increase in the phase-space density of the solution at $v \cong -1.5\times10^{-9}$ cm/s and a decrease in phase-space density at $v > -1.0\times10^{-9}$ cm/s.

VI. DISCUSSION AND CONCLUSIONS

Modeling of FAST satellite observations of the parallel electric fields and the accompanying electron and ion distributions provides solid support to the idea that the parallel electric field at the ionospheric boundary of the auroral cavity is self-consistently supported as an oblique double layer. Numerical solutions to the Vlasov–Poisson equations indicate that the observed electric fields, electron distributions, and ion distributions are in accordance with the oblique

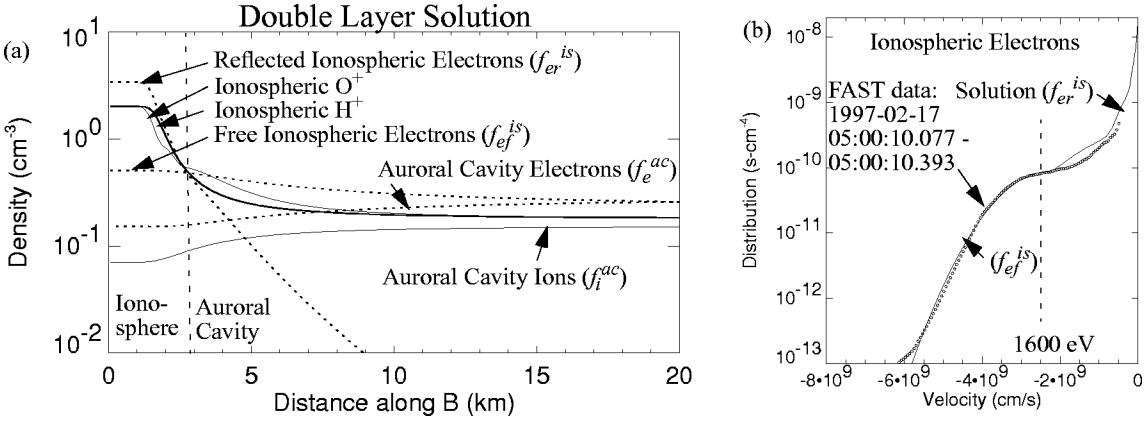

FIG. 8. The self-consistent numerical solution to an oblique, asymmetric double layer using fits to observed distributions. (a) The densities as a function of z, the distance along **B**. (b) The derived electron distribution. In this example, electrons are assumed to be infinitely magnetized. The ions are assumed to 50% be weakly magnetized O^+ and 50% H^+. The polarization drift and the **E×B** drift in the O^+ distributions are treated as perturbations using Eq. (8).

double layer interpretation. There are several interesting features that emerge from the observationally-driven numerical solution. The significant gradient in plasma density (a change of nearly a factor of 10) across the double layer results in an asymmetric electric field signature. The double layer has a strong, confined positive layer on the ionospheric side and a moderate, extended negative charge layer on the auroral cavity side. The structure of the double layer is almost entirely determined by the ionospheric populations since the magnetospheric species have only a minor contribution to the net charge density.

The electron distribution on the ionospheric side includes scattered and reflected primaries, auroral secondaries, and a cold population. The cold (3 eV) population, determined from the double layer solution, is almost entirely reflected in the first ~ 1 km of the double layer, creating a thin layer of a large positive charge. The hotter population (f_{ef}^{is}), consisting of scattered primaries, auroral secondaries, and energetic ionospheric photoelectrons, penetrates the double layer and makes up a substantial fraction ($\sim 25\%$ to 50%) of the electron density in the auroral cavity.

The ionospheric ions are observed to have a drift that satisfies the Bohm condition. They are accelerated into a beam as they penetrate the double layer and wave–particle interactions rapidly heat the ions parallel to **B**. The interplay of the accelerated ion beam and the free electron population (reflected auroral electrons, electron secondaries, and scattered primaries) creates an extended, relatively weak negative charge layer. Because of the dominant role of the ionospheric distributions, the auroral cavity distributions are not required by themselves to satisfy the Bohm condition. The ion and electron pressures are in balance to lowest order, so the Langmuir condition may be satisfied in a stationary frame.

The asymmetric shape of the electric field signal and a strong gradient in plasma density is seen in almost all direct observations of the parallel electric field. The above numerical analyses demonstrate that the asymmetric shape of the electric field signal is in accordance with the strong density gradient. The relatively strong, localized positive charge layer on the ionospheric side scales more closely to the ionospheric Debye length whereas the extended, moderate negative charge layer scales with the Debye length in the auroral cavity.

The electric field observations in the example we studied, however, do not entirely support the planar model of an oblique double layer. Under a planar model, the two components, $E_{\perp}$ and $E_{\parallel}$, should be highly correlated. Such a good correlation is seen in roughly one half of the ten events identified by Polar and FAST. It is possible that the ionospheric boundary may also form ''stair step'' potential structure. In this case, the two- or three-dimensional Laplacian operator must be used in a Vlasov–Poisson solution.

The electron acceleration from the double layer can result in an unstable electron distribution and intense lower hybrid and quasi-dc turbulence. These waves may interact with the double layer through ion heating. The intense electrostatic wave turbulence heats the ions on the ionospheric boundary into a drifting ''conic'' distribution. The magnetic mirror force then accelerated the distribution into the double layer. Ion heating may critically affect the double layer solution and therefore needs further investigation.

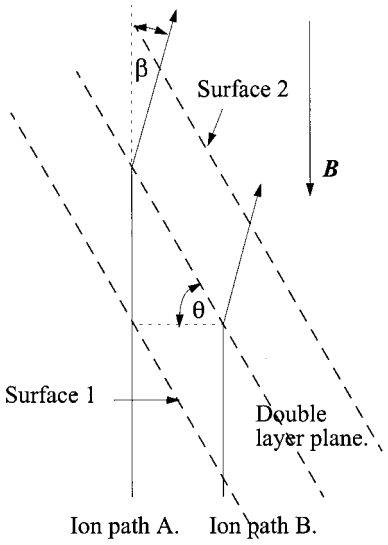

FIG. 9. The deflection of the ion paths due to the polarization drift result in a density perturbation that depends on the deflection angle β. The thick dashed lines represent the plane of the double layer and the solid lines represent two different ion paths.

The solutions match the observations best if we account for the polarization drift and **E×B** drift of O^+ and include a mixture of $\sim 70\%$ H^+ and 30% O^+. The streaming ion beam emerging into the auroral cavity may also be unstable. In spite of the large acceleration relative to the initial thermal speed, a strong instability is not expected from the ion beam interaction with the ambient ion population in the auroral cavity (1 keV–5 keV plasma sheet ions). The intense low-frequency waves, however, are observed to coexist with the parallel electric field of the double layer indicating a shear instability, an ion–ion (O^+/H^+) two-stream instability, or another wave-growth mechanism. This analysis suggests an oblique double layer as the lowest-order solution, but a fully dynamic, two-dimensional analysis is needed for a better understanding.

ACKNOWLEDGMENTS

This work is supported by NASA Grants No. NAG5-120026, No. NAG5-3596, and NSF Grant No. ATM-0202564.

APPENDIX: ION POLARIZATION DRIFT

We derive the density change from the ion polarization drift using a geometric argument and assuming that the guiding center approximation is valid, that is, the conditions for the polarization drift hold. As described by Swift,[7] the guiding center approximation also breaks down as ϵ [Eq. (5)] approaches unity, so a full kinetic solution is ideal.

Figure 9 sketches the basic geometry and defines some parameters. The argument goes as follows. The guiding centers of ions A and B will follow the magnetic field until they reach the double layer plane. Within the double layer, the paths are deflected by angle β (variable) from the local equi-

potential plane as they experience acceleration and a polarization drift. In the plane of the double layer, the flux of the ions through Surface 1 must be the same as that through Surface 2. The ions experience the identical potentials along the double layer plane, so flux conservation becomes

$$n_u \nu_u \cos(\theta) = n_p \nu_p \cos(\theta - \beta), \tag{A1}$$

where n_u and ν_u are the unperturbed density and velocity (that is, the density and velocity expected if there were no polarization or $\mathbf{E}\times\mathbf{B}$ drift) and n_p and ν_p are the density and velocity perturbed by the polarization drift. Isolating, the density perturbation due solely to the perturbation drift, we calculate

$$\frac{n_p \nu_p}{n_u \nu_u} = \frac{\cos(\theta)}{\cos(\theta - \beta)} = \frac{\sqrt{1+\tan^2(\beta)}}{1+\tan(\theta)\tan(\beta)}. \tag{A2}$$

The deflection angle β can vary and is derived from the guiding center motion of the polarization drift which can be described as

$$\frac{dx}{dt} = \frac{e}{M\omega_{ci}^2}\frac{dE_x}{dt} = \frac{e}{M\omega_{ci}^2}\left(\frac{dE_x}{dx}\frac{dx}{dt} + \frac{dE_x}{dz}\frac{dz}{dt}\right). \tag{A3}$$

From Eq. (A3), the ion trajectories can be described by

$$\frac{dx}{dz} = \frac{e}{M\omega_{ci}^2}\frac{dE_x}{dz} \Bigg/ \left(1 - \frac{e}{M\omega_{ci}^2}\frac{dE_x}{dx}\right). \tag{A4}$$

For convenience, we use the relation

$$\frac{dE_x}{dx} = \frac{dE_x}{dz}\tan(\theta), \tag{A5}$$

and, as described in Eq. (9), let

$$\epsilon = \frac{e}{M\omega_{ci}^2}\frac{dE_x}{dx}. \tag{A6}$$

Equation (A3) becomes

$$\frac{dx}{dz} = \frac{\epsilon}{\tan(\theta)(1-\epsilon)} = \tan(\beta), \tag{A7}$$

where β is the instantaneous angle of deflection.

Combining Eqs. (A2) and (A7), we get

$$\frac{n_p \nu_p}{n_u \nu_u} = \sqrt{(1-\epsilon)^2 + \epsilon^2 \cot^2(\theta)} \times \sqrt{\left(1 - \frac{e}{M\omega_{ci}^2}\frac{dE_x}{dx}\right)^2 + \left(\frac{e}{M\omega_{ci}^2}\frac{dE_x}{dz}\right)^2}. \tag{A8}$$

[1] R. E. Ergun, L. Andersson, D. S. Main, Y.-J. Su, C. W. Carlson, J. P. McFadden, and F. S. Mozer, Phys. Plasmas **9**, 3685 (2002).
[2] F. S. Mozer and C. A. Kletzing, Geophys. Res. Lett. **25**, 1629 (1998).
[3] L. P. Block, Cosm. Electrodyn. **3**, 349 (1972).
[4] J. R. Kan, J. Geophys. Res. **80**, 2089 (1975).
[5] D. W. Swift and J. R. Kan, J. Geophys. Res. **80**, 985 (1975).
[6] D. W. Swift, J. Geophys. Res. **80**, 2096 (1975).
[7] D. W. Swift, J. Geophys. Res. **84**, 6427 (1979).
[8] M. A. Raadu, Phys. Rep. **178**, 25 (1989).
[9] P. H. Reiff, H. L. Collin, J. D. Craven, J. L. Burch, J. D. Winningham, E. G. Shelley, L. A. Frank, and M. A. Friedman, J. Geophys. Res. **93**, 7441 (1988).
[10] J. L. Burch, Adv. Space Res. **8**, 353 (1988).
[11] C. Gurgiolo and J. L. Burch, J. Geophys. Res. **93**, 3989 (1988).
[12] R. E. Ergun, C. W. Carlson, J. P. McFadden, F. S. Mozer, and R. J. Strangeway, Geophys. Res. Lett. **27**, 4053 (2000).
[13] G. Knorr and C. K. Goertz, Astrophys. Space Sci. **31**, 209 (1974).
[14] H. Schamel and S. Bujarbarua, Phys. Fluids **26**, 190 (1983).
[15] M. A. Raadu and J. J. Rasmussen, Astrophys. Space Sci. **144**, 43 (1988).
[16] S. Torvén and D. Andersson, J. Phys. D **12**, 717 (1979).
[17] S. Torvén and L. Lindberg, J. Phys. D **13**, 2285 (1980).
[18] R. E. Ergun, C. W. Carlson, J. P. McFadden, F. S. Mozer, Y.-J. Su, L. Andersson, D. L. Newman, M. V. Goldman, and R. J. Strangeway, Phys. Rev. Lett. **87**, 045003 (2001).
[19] F. S. Mozer, C. W. Carlson, M. K. Hudson, R. B. Torbert, B. Parady, J. Yatteau, and M. C. Kelley, Phys. Rev. Lett. **38**, 292 (1977).
[20] J. E. Borovsky and G. Joyce, J. Plasma Phys. **29**, 45 (1983).
[21] M. K. Hudson, W. Lotko, I. Roth, and E. Witt, J. Geophys. Res. **88**, 916 (1983).
[22] V. V. Gavrishchaka, G. I. Ganguli, W. A. Scales, S. P. Slinker, C. C. Chaston, J. P. McFadden, R. E. Ergun, and C. W. Carlson, Phys. Rev. Lett. **85**, 4285 (2000).
[23] O. Penrose, Phys. Fluids **3**, 411 (1960).
[24] Y. T. Chiu and M. Schultz, J. Geophys. Res. **83**, 629 (1978).
[25] S. Knight, Planet. Space Sci. **21**, 741 (1973).